Pramana – J. Phys. (2019) 92:50
https://doi.org/10.1007/s12043-018-1716-9

Beyond the conventional collisional absorption of laser light in under-dense plasma: A particle-in-cell simulation study

M KUNDU[1,2]

[1]Institute for Plasma Research, Bhat, Gandhinagar 382 428, India
[2]Homi Bhaba National Institute, Training School Complex, Anushakti Nagar, Mumbai 400 094, India
E-mail: mkundu@ipr.res.in

MS received 3 January 2018; revised 12 March 2018; accepted 4 September 2018;
published online 15 February 2019

Abstract. Collisional absorption of laser light in an under-dense plasma is studied by particle-in-cell (PIC) simulation with Monte Carlo binary Coulomb collisions between charge particles. For a given plasma thickness of a few times the wavelength of 800 nm laser, fractional absorption (α) of the laser light due to Coulomb collisions (mainly between electrons and ions) is calculated at different electron temperature T_e with a total velocity $v = (v_{th}^2 + v_0^2/2)^{1/2}$ dependent Coulomb logarithm $\ln \Lambda(v)$, where v_{th} and v_0 are thermal and ponderomotive velocity of an electron. In the low-temperature regime ($T_e \lesssim 15$ eV), it is found that α increases with increasing laser intensity I_0 up to a maximum corresponding to an intensity I_c, and then it drops (approximately) obeying the conventional scaling of $\alpha \propto I_0^{-3/2}$ when $I_0 > I_c$. Such a non-conventional increase of α with I_0 in the low-intensity regime was demonstrated earlier in experiments, and recently explained by classical and quantum models [*Phys. Plasmas* **21**, 13302 (2014); *Phys. Rev. E* **91**, 043102 (2015)]. Here, for the first time, we report this non-conventional collisional laser absorption by PIC simulation, thus bridging the gap between models, simulations, and experimental findings. Moreover, electron energy distributions naturally emanating during the laser interaction (in PIC simulations) are found to be anisotropic and non-Maxwellian in nature, leading to some deviations from the earlier analytical predictions.

Keywords. Collisional absorption; particle-in-cell simulation; under-dense plasma.

PACS No. 52.50.Jm

1. Introduction

One of the main objectives of the researchers working in the field of laser–plasma interaction (LPI) is to couple more laser energy with the plasma (or matter) so as to obtain more energetic charge particles or intense radiations. Therefore, it is of prime importance to know the underlying physical process (collisional and collisionless) by which laser energy is coupled to the plasma during the interaction. Earlier experiments [1–4] and theoretical studies [5–9] have reported various absorption processes, e.g., linear resonance [10], anharmonic resonance [4,11–17], Brunel heating [18], $\mathbf{J} \times \mathbf{B}$ heating [19] etc., which often depend on parameters of the laser, and the plasma. For example, while passing through under-dense plasma (where plasma frequency ω_p is less than the laser frequency ω), an intense p-polarised short laser pulse can be absorbed by exciting wake-fields and instabilities [7–9]. On the other hand, in an overdense plasma with an under-dense pedestal, linear resonance absorption (LR) of p-polarised light may occur by meeting the resonance condition $\omega_p = \omega$ in a specific location of the density gradient. Most often p-polarised light is used by experimentalists because of its ability to drive the plasma more efficiently, and relatively less attention is paid for s-polarised light. However, absorption of both s- and p-polarised light in plasma may happen through the electron–ion collision [7,8,20,21] known as inverse bremsstrahlung (IB) if laser intensity is below 10^{17} W cm^2. In this case, laser energy is initially coupled to electrons and a part of this energy is transferred to plasma ions, mainly via electron–ion Coulomb collisions in a time scale on the order of the inverse of the electron–ion collision frequency ν_{ei}.

In this work, we concentrate on the absorption of an s-polarised laser light in a homogeneous, under-dense plasma-slab due to IB, because collisional and collisionless absorption processes are coupled together for

a p-polarised light where it is difficult to know what fraction of the collisional absorption contributes to the total absorption. We are also motivated by earlier experimental results [8,22] of collisional absorption with s-polarised light which shows that fractional absorption α of light (i.e., ratio of the absorbed energy to the incident laser energy) non-conventionally increases initially with increasing laser intensity I_0 up to a maximum value about an intensity I_c, and then it drops nearly obeying the conventional scaling [7,8] of $\alpha \propto I_0^{-3/2}$.

Although there are numerous analytical models [20–42] which directly or indirectly describe conventional (standard) collisional absorption neglecting the effect of background plasma, less attempts were made to examine the aforementioned non-conventional collisional absorption (NCA). Recently, NCA has been explained in the low-temperature regime ($T_e \lesssim 15$ eV) by postulating a total velocity dependent Coulomb logarithm $\ln \Lambda(v)$ (where $v = (v_{th}^2 + v_0^2/2)^{1/2}$, v_{th} and v_0 are the thermal and ponderomotive velocity) in the ballistic model of electron–ion collision frequency ν_{ei} [32,43] and more rigorous kinetic model [44]. However, the extent of validity of these analytical models are not yet known which can only be answered numerically with self-consistent dynamics of plasma background under the laser irradiation. To achieve this goal, we have developed a one-dimensional electromagnetic particle-in-cell code (henceforth we call it EMPIC1D) where variation of physical quantities (charge density, current density, electromagnetic fields) depend only on the one spatial coordinate along the laser propagation direction while considering all three velocity components of charge particles. In a PIC simulation, a reduced number of computational particles is used to represent plasma, instead of the actual number of physical particles [45,46]. This technique reduces the computational load, and enables one to study the dynamics of an actual physical system of a large number of charge particles. Sizes of these PIC particles (computational particles) are typically on the order of a numerical grid, they can pass through each other during the interaction, and Coulomb collisions do not naturally happen [47–50]. For this reason, Coulomb collisions are explicitly added in all PIC codes. To include Coulomb collision in our EMPIC1D code, a Monte Carlo (MC) technique proposed by Takizuka and Abe [48] is adopted. Recently, this scheme was used in the PARASOL electrostatic PIC code [49] to study kinetic effects in tokamak plasmas. EMPIC1D conserves total energy and total linear momentum before and after a collision event in the velocity space.

With the EMPIC1D code, for the first time, we prove the aforementioned NCA in an under-dense plasma in the low-temperature and low-intensity regime similar to the earlier analytical works [43,44]. However, the electron energy distributions emanating from the laser interaction with the plasma (in the current PIC simulations) are found to be anisotropic and non-Maxwellian which is also a new finding of this work and cannot be captured by previous theories. Plasma is assumed to be pre-ionised. Laser intensity is kept below $10^{18}\,\mathrm{W\,cm^{-2}}$ so that relativistic effects are less important. For convenience, atomic units (a.u.) are used unless mentioned explicitly, i.e., $|-e| = m = 4\pi\epsilon_0 = \hbar = 1$, where $|e|$ and m are the electronic charge and mass, ϵ_0 is the permittivity of the free space and $\hbar$ is the reduced Planck constant.

This article is organised in the following manner. Details of the EMPIC1D code is given in §2. Study of collisional absorption of s-polarised light in an under-dense plasma slab showing NCA is reported in §3. A summary is given in §4.

2. Details of the PIC code

In PIC simulation, a collection of physical particles is represented by a computational particle so that the charge to mass ratio q/m of the computational particle remains the same as that of a physical particle. The following Maxwell–Lorentz system of equations (in the normalised form) is solved numerically after the discretisation in space and time:

$$\frac{\partial \bar{\mathbf{B}}}{\partial t} = -c\nabla \times \mathbf{E}, \tag{1}$$

$$\frac{\partial \mathbf{E}}{\partial t} = c\nabla \times \bar{\mathbf{B}} - 4\pi \mathbf{J}, \tag{2}$$

$$\dot{\mathbf{p}} = q\left(\mathbf{E_p} + \mathbf{v} \times \frac{\bar{\mathbf{B}}_p}{c}\right). \tag{3}$$

Here, $\mathbf{E}, \bar{\mathbf{B}}$ are the electric and magnetic parts of the electromagnetic field, $\mathbf{p}$ is the particle momentum corresponding to its velocity $\mathbf{v}$ and position $\mathbf{r}$ at a time t. $\mathbf{J}$ is the current density vector, c is the speed of light in the free space. The scaling $\bar{\mathbf{B}} = c\mathbf{B}$ connects the actual magnetic field $\mathbf{B}$ with the scaled magnetic field $\bar{\mathbf{B}}$. The other equations, namely, $\nabla \cdot \bar{\mathbf{B}} = 0$ and the Gauss's law $\nabla \cdot \mathbf{E} = 4\pi\rho$ are not explicitly solved in a standard multidimensional PIC scheme, thus saving a substantial amount of computer time. However, $\nabla \cdot \bar{\mathbf{B}} = 0$ is ensured by choosing a staggered grid, called Yee mesh. The charge and current conservation follows from $\partial\rho/\partial t + \nabla \cdot \mathbf{J} = 0$, thus ensuring $\nabla \cdot \mathbf{E} = 4\pi\rho$. Note that $\mathbf{E}$, $\bar{\mathbf{B}}$, $\mathbf{J}$, ρ are calculated on the grid points. Therefore, $\mathbf{E}, \bar{\mathbf{B}}$ fields are interpolated to obtain the corresponding fields $\mathbf{E}_p, \bar{\mathbf{B}}_p$ at the particle (particle charge q and mass m) position $\mathbf{r}$ using the linear weighting scheme, and

the Lorentz equation (3) is solved using the standard leap-frog method. The advantage of the scaling $\bar{\mathbf{B}} = c\mathbf{B}$ is that, it reduces eqs (1) and (2) identical in form in the free space (i.e., when $\mathbf{J} = 0$) and the amplitudes of $\mathbf{E}$, $\bar{\mathbf{B}}$ becomes comparable. From now onwards, for convenience, we shall write $\mathbf{B}$ instead of $\bar{\mathbf{B}}$ unless mentioned explicitly.

2.1 *Simplification in one dimension*

Let us consider an *s*-polarised light (propagating in y-direction) with transverse field components E_z, B_x. The physical quantities (e.g., charge density, current density and electromagnetic fields) are assumed to depend only on the space coordinate y, while retaining all the three velocity components (v_x, v_y, v_z) of the particles. Components of eqs (1) and (2) reads as

$$\frac{\partial B_x}{\partial t} = -c\frac{\partial E_z}{\partial y}, \tag{4}$$

$$\frac{\partial E_z}{\partial t} = -c\frac{\partial B_x}{\partial y} - 4\pi J_z(t, y), \tag{5}$$

$$\frac{\partial E_y}{\partial t} = -4\pi J_y(t, y). \tag{6}$$

Equation (6) gives longitudinal component of the electric field E_y in our case. It is important to mention that, the numerical implementation of our PIC code is a little different from some of the traditional 1D-PIC codes, namely, EM1BND [45], LPIC++ [51], but closely follow the implementation in PIC codes PSC [52]. In EM1BND [45] and LPIC++ [51], by performing addition and subtraction of eqs (4) and (5), and writing $\psi_\pm = E_z \pm B_x$ one finds $(\partial_t \pm c\partial_y)\psi_\pm = -4\pi J_z(t, y)$, where $\psi_\pm$ can be recognised as the two propagating solutions of the wave equation. The advantage in this traditional procedure [45,51] is that the partial derivative $(\partial_t \pm c\partial_y)$ can be written in terms of the total derivative in time with respect to an observer moving at a speed $\pm c$, leading to

$$\frac{\mathrm{d}\psi_\pm}{\mathrm{d}t} = -4\pi J_z(t, y). \tag{7}$$

For a given J_z, eq. (7) is solved as an ordinary differential equation (ODE) to obtain transverse fields $E_z = (\psi_+ + \psi_-)/2$, $B_x = (\psi_+ - \psi_-)/2$ on the grid. It also allows larger time step $\Delta t = \Delta y/c$. The disadvantage is that, the longitudinal component E_y is obtained by solving the Poisson's equation $\partial E_y/\partial y = 4\pi\rho$ explicitly (not from eq. (6)), and it needs a separate algorithm to solve the transverse components. Moreover, this traditional scheme is hard to extend in multidimensional case. In our EMPIC1D code, we use finite difference in time domain (FDTD) method for the solution of all field components (both traverse and longitudinal), instead of the aforementioned traditional addition–subtraction method. Thus, we use only one kind of algorithm for E_z, B_x, E_y which is extendable to PIC simulations in higher dimensions as in ref. [52]. Using FDTD procedure on the Yee mesh, and assuming $t = n\Delta t$, $y = k\Delta y$, eqs (4)–(6) can be written as

$$\frac{B^{n+1}_{x,\,k+1/2} - B^{n}_{x,\,k+1/2}}{\Delta t} = -c\frac{E^{n+1/2}_{z,\,k+1} - E^{n+1/2}_{z,\,k}}{\Delta y} \tag{8}$$

$$\frac{E^{n+1/2}_{z,\,k+1} - E^{n-1/2}_{z,\,k+1}}{\Delta t} = -c\frac{B^{n+1}_{x,\,k+1/2} - B^{n+1}_{x,\,k-1/2}}{\Delta y} - 4\pi J^{n+1/2}_{z,\,k+1} \tag{9}$$

$$\frac{E^{n+1/2}_{y,\,k+1} - E^{n-1/2}_{y,\,k+1}}{\Delta t} = -4\pi J^{n+1/2}_{y,\,k+1}. \tag{10}$$

To ensure numerical stability we take $c\Delta t/\Delta y = 1/2$, which decides the time step Δt for a chosen grid size Δy. The dispersion due to the FDTD discretisation is minimised by choosing sufficient number of spatial grids (minimum 40 is taken) per wavelength of light. The current density $\mathbf{J}$ due to the motion of charge particles is computed using the 'explicit current conserving scheme' by Umeda *et al* [53] which satisfies $\partial\rho/\partial t + \nabla \cdot \mathbf{J} = 0$. Thus, we avoid explicit solution of the Poisson's equation to obtain E_y. We use 'perfectly matched layer' (PML) absorbing boundary condition [54] for the electromagnetic fields. For charge particles, however, depending upon physical situations, absorbing, periodic, and reflecting boundary conditions are used.

2.2 *Binary collision model*

In the PIC simulation, as discussed already, particles may pass through each other during their close encounter and collision effects are omitted. To implement binary collision in the EMPIC1D code we have followed the Monte Carlo scheme given by Takizuka and Abe [48] and also the work by Ma *et al* [50] and Sentoku *et al* [47]. The main approximation of binary collision is that at a given instant only two particles will collide, and the effect of collision arises due to the cumulative effect of many small-angle binary collisions. Within a computational cell, particles are paired randomly (ion–ion, ion–electron, electron–electron) and then collision is performed between every pair. The maximum impact parameter in a fully ionised quasineutral plasma being of the order of the Debye length, the maximum size of the collision grid is also restricted to the Debye length. Collision event takes place in the velocity space, which means that the velocity components of the particles change but

the coordinates are not influenced at that time. The post-collision velocities are obtained by going to the centre of mass (COM) frame of the respective collision pairs and then back to the laboratory frame. Due to collision, during a small time interval Δt_c (which is sufficiently small compared to the mean relaxation time), the direction of velocities of the colliding particles changes but not their magnitudes. For instance, we consider a system of two particles from two species α and β having velocities v_α and v_β, masses m_α and m_β, densities n_α and n_β, and charges e_α and e_β. At a given instant t, the effect of collision leads to the rotation of the relative velocity $\mathbf{u} = \mathbf{v}_\alpha - \mathbf{v}_\beta$ in the COM frame of the two particles. The relative velocity $\mathbf{u}' = \mathbf{v}'_\alpha - \mathbf{v}'_\beta$ after the collision (prime represents quantities after collisions) in the COM frame, and the rotation of the velocity vector $\mathbf{u} \to \mathbf{u}'$ can be described by the scattering angle Θ and the azimuth angle Φ which are chosen randomly for a given pair (α, β). In order to find Θ, a parameter δ is introduced such that $\delta = \tan(\Theta/2)$. The variable δ is chosen randomly from a Gaussian distribution such that its mean is zero, and the corresponding variance [48–50] is $\langle\delta^2\rangle = (e_\alpha^2 e_\beta^2 n_L \ln\Lambda)\Delta t_c/(8\pi\epsilon_0^2 m_{\alpha\beta}^2 u^3)$. Here n_L is the minimum density between n_α and n_β, $m_{\alpha\beta} = m_\alpha m_\beta/(m_\alpha + m_\beta)$ is the reduced mass and $\ln\Lambda$ is the Coulomb logarithm. $\ln\Lambda$ should include the response of electrons to the laser field strength E_0 and the frequency ω. The necessary modification of $\ln\Lambda$ with laser field will be discussed later. The deflection angle Θ is calculated by using Box–Muller method with distribution $p(\delta)\mathrm{d}\delta = (1/\langle\delta^2\rangle)\exp(-\delta^2/2\langle\delta^2\rangle)\delta\mathrm{d}\delta$ as given in refs [55,56], $\Theta = 2\arctan\sqrt{-2\langle\delta^2\rangle\ln(1-R_1)}$, where R_1 is a uniform random number between 0 and 1. The azimuth angle Φ is chosen as $\Phi = 2\pi R_2$, with R_2 being a uniform random number between 0 and 1. The change in velocity components in the laboratory frame can be calculated as [48]

$$\Delta u_x = \frac{u_x}{u_\perp}u_z \sin\Theta\cos\Phi - \frac{u_y}{u_\perp}u\sin\Theta\sin\Phi - u_x(1-\cos\Theta), \tag{11}$$

$$\Delta u_y = \frac{u_y}{u_\perp}u_z \sin\Theta\cos\Phi + \frac{u_x}{u_\perp}u\sin\Theta\sin\Phi - u_y(1-\cos\Theta), \tag{12}$$

$$\Delta u_z = -u_\perp \sin\Theta\cos\Phi - u_z(1-\cos\Theta), \tag{13}$$

where

$$u_\perp = \sqrt{u_x^2 + u_y^2}. \tag{14}$$

When $u_\perp = 0$, we take

$$\Delta u_x = u\sin\Theta\cos\Phi, \quad \Delta u_y = u\sin\Theta\sin\Phi, \quad \Delta u_z = -u(1-\cos\Theta). \tag{15}$$

The final post-collision velocities in the laboratory frame reads as

$$\mathbf{v}_\alpha(t+\Delta t_c) = \mathbf{v}_\alpha(t) + (m_{\alpha\beta}/m_\alpha)\Delta\mathbf{u}, \tag{16}$$

$$\mathbf{v}_\beta(t+\Delta t_c) = \mathbf{v}_\beta(t) - (m_{\alpha\beta}/m_\beta)\Delta\mathbf{u}. \tag{17}$$

3. Absorption in an under-dense plasma

The above collision scheme is incorporated in the EMPIC1D code to study collisional absorption of light incident normally on an under-dense plasma slab of uniform density. The simulation domain consists of $N_g = 500$ computational cells with the plasma slab at the centre. Initially, each computational cell contains equal number of electrons and ions so that plasma is charge neutral. The temporal profile of the laser pulse (at the left boundary, y_l) is chosen as

$$E_z(t, y_l) = E_0 \begin{cases} \sin^2(\omega t/2n_c)\cos(\omega t); & 0 < t < n_c T \\ 0; & t > n_c T, \end{cases} \tag{18}$$

where n_c is the number of cycles and $T = 2\pi/\omega$ is the laser period. The pulse is numerically excited at $y = y_l$, propagates in free space, then strikes the plasma slab. The intensity, wavelength, number of cycles, the duration of pulse and the width L_p of the plasma slab can be varied as desired. Accordingly, the length of the computational domain and the number of computational cells N_g are also adjusted. We choose the laser wavelength $\lambda = 800$ nm with $n_c = 4$-cycles and the total duration ≈ 30 fs. The size of a computational cell is chosen as $\Delta = 200$ a.u. which yields the PIC time step $\Delta t_\mathrm{PIC} = 0.73$ a.u. Length of the plasma is chosen as $L_\mathrm{p} \approx 1.32\lambda$ with a density $\rho/\rho_c \approx 0.136$. Temperature of ions is kept fixed in all simulations at $T_\mathrm{i} = 5$ eV while temperatures of electrons are kept fixed at $T_\mathrm{e} = 5, 10, ..., 50, 100$ eV for a given laser intensity. The chosen value of T_i, however, is found to have negligible effect on the overall results of collisional absorption. These parameters are kept fixed during a simulation run. To simulate collisional absorption in a laser field, the Coulomb logarithm should not be the same as that of ordinary collisions, because it does not include the laser field parameters. Earlier, Djaoui and Offenberger [57] have mentioned possible choices of total velocity, i.e., $v^2 = v_\mathrm{th}^2 + v_0^2/6$, $v^2 = v_\mathrm{th}^2 + v_0^2$, $v^2 = v_\mathrm{th}^2 + v_0^2/3$ etc. (see also refs [22,23,37,38]) for different models of ν_ei. In fact, various forms of $\ln\Lambda$ are

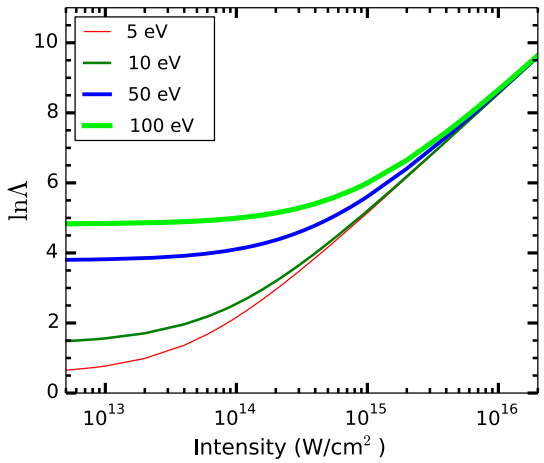

Figure 1. ln Λ vs. laser intensity for $T_e = 5$, 10, 50 and 100 eV with total velocity $v = (v_{th}^2 + v_0^2/2)^{1/2}$ and charge density $\rho = 0.136\rho_c$.

still debated [34,43,44]. As there is no unique model of ln Λ in a laser field, we use a modified form [32,37,43],

$$\ln \Lambda = 0.5 \ln[1 + (b_{max}/b_\perp)^2], \tag{19}$$

where $b_{max} = v/\max(\omega, \omega_p)$, $b_\perp = 1/v^2$, with $v^2 = v_{th}^2 + v_0^2/2$ as the total velocity. The effect of laser field is incorporated through the ponderomotive velocity $v_0 = E_0/\omega$. The physical mechanism of the dependence of ln Λ on the laser field strength (or intensity) can be argued due to the reorientation of the momentum of a colliding electron with an ion not only due to the thermal component of its velocity (which is conventionally taken) but also due to the momentum imparted to it through the laser field strength. Figure 1 shows the non-uniform variation of ln Λ vs. intensity (19) for different T_e.

From the simulation, we record total kinetic energy ke gained by the particles, the electric part $ee = \sum_1^{N_g} E_j^2 \Delta/8\pi$ and the magnetic part $me = \sum_1^{N_g} B_j^2 \Delta/8\pi$ of the electromagnetic energy at every time step, giving the total energy $te = ke + ee + me$. Figure 2 shows temporal variation of various energies at intensity $I_0 = 5 \times 10^{14}$ W cm^2 for two cases: (a) without collision and (b) with collision between electrons and ions. In figures 2a and 2b for the initial time upto $t/T \approx 3$, all energies ee, me and te increase sharply as the laser pulse is entering the simulation domain. For $t/T \approx 3 - 4$ the values of ee, me remain almost constant and te reaches a maximum because the entire pulse has appeared in the simulation domain. The pulse strikes the plasma slab about $t/T \approx 4$, and only after this time, for $t/T = 4 - 7.5$, ke first increases and then drops with the corresponding drop and increase in ee and me while te remains conserved at the highest value. After

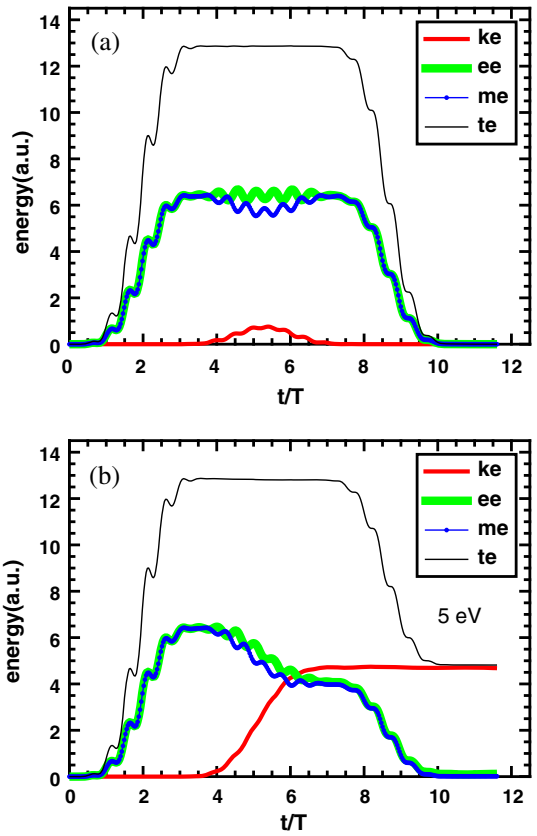

Figure 2. Different energy profiles (kinetic energy ke, electric part $ee = \sum E_j^2 \Delta/8\pi$, magnetic part $me = \sum B_j^2 \Delta/8\pi$ of the electromagnetic energy, and the total energy $te = ke + ee + me$) vs. normalized time t/T for s-polarised light interacting with an under-dense plasma of $\rho \approx 0.136\rho_c$. (**a**) Without collision, energy is not absorbed finally and (**b**) with collision, laser energy is absorbed, and transferred to the particle kinetic energies (see $ke \neq 0$) at the end of the interaction.

$t/T \approx 7.5$, values of ee, me and te sharply drop because the laser pulse is leaving the finite simulation domain, and gets absorbed (artificially) in the right boundary. The constant value of total energy, when the entire pulse is inside the computational box (for $t/T = 3 - 7.5$), indicates conservation of energy in the simulation. In figure 2a, without collision, ke reaches a maximum value, and finally drops to zero before $t/T \approx 7.5$. This is expected, because particles cannot retain this energy, and finally gives back to the electromagnetic fields (which is also evident from the corresponding drop and rise of ee and me between $t/T = 4 - 7.5$), resulting no net absorption. However, when collision is taken into account (in figure 2b) ke increases monotonically in time starting at $t/T \approx 4$ (with a corresponding drop in ee and me, meaning absorption of the pulse), and reaches a non-zero saturation value around $t/T = 6.8$ much before the pulse has left the simulation box. ke

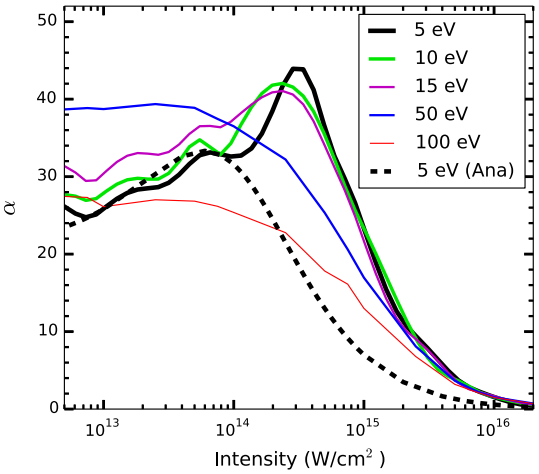

Figure 3. Fractional absorption vs. peak laser intensity for s-polarised light interacting with an under-dense plasma as in figure 2 for $T_e = 5, 10, 15, 50, 100$ eV (numerical, solid line) and $T_e = 5$ eV (analytical, dashed line, using eq. (21)).

does not drop to zero even after the pulse is over which clearly shows that s-polarised light can be absorbed due to collisions and the laser energy can be transferred to the charge particles.

We now find the nature of collisional absorption by varying the intensity of the laser pulse for a given initial temperature T_e. In reality, T_e should also vary during the interaction. The other parameters, such as plasma thickness L_p, plasma density ρ and ion temperature T_i are kept constant as earlier. Figure 3 shows fractional absorption α, defined as the ratio of the final kinetic energy retained in the particles to the maximum of te (which is actually the total energy in the laser pulse), vs. the peak intensity for $T_e = 5 - 100$ eV. It is seen that, for higher temperatures $T_e > 20$ eV, α initially remains almost constant (or vary slowly) upto a certain value $I_c \approx 6 \times 10^{13}$ W cm^{-2} of the peak intensity, and then decreases gradually for intensities $I_0 > I_c$. This represents the conventional result of collisional absorption reported in earlier works [20,21,58] with $\ln\Lambda$ independent of the ponderomotive velocity $v_0 = E_0/\omega$. However, when $T_e < 20$ eV, it is found that α initially increases with the intensity, reaches a maximum value about an intensity $I_c \approx 5 \times 10^{14}$ W cm^{-2}, then drops similar to the high temperature case. Such a non-conventional variation (initial increase followed by a drop) of fractional absorption vs. the laser intensity was reported experimentally with normally incident s-polarised light (of wavelengths 800 nm [8] and 268 nm [22]) on an under-dense plasma with the peak absorption more than 30%. Incorporating a total velocity-dependent $\ln\Lambda$ in the EMPIC1D code for the first time we find similar non-conventional variation of collisional absorption in the low-temperature and low-intensity regime. Our results indicate that absorption due to collisional process can be as high as 40% depending upon plasma and laser parameters.

For the shake of completeness, PIC results are compared (dashed line in figure 3) using $\ln\Lambda$ of eq. (19) in the ballistic model [32,43] of time-dependent ν_{ei}, i.e.,

$$\nu_{ei}(t) = (\omega_p^2 \ln\Lambda / v_{os}^3(t))\left[\mathrm{erf}(u(t)) - \frac{2}{\sqrt{\pi}} u(t) e^{-u(t)^2}\right], \tag{20}$$

where $u(t) = v_{os}(t)/\sqrt{2}v_{th}$ and $v_{os}(t)$ is the oscillation velocity of the electron in the laser field. Averaging $\nu_{ei}(t)$ over a laser period leads to average $\bar{\nu}_{ei}$ and fractional absorption

$$\alpha = 1 - \exp(-2\kappa_i L_p) \tag{21}$$

of a continuous light of frequency ω in an under-dense plasma slab [7,8] at normal incidence. Here $\kappa_i = (\rho/\rho_c)\bar{\nu}_{ei}/v_g$, and $v_g = c\sqrt{1-\rho/\rho_c}$ is the group velocity of light. Analytical result (dashed line) using eq. (21) at $T_e = 5$ eV shows good agreement with the EMPIC1D result for intensities $<10^{14}$ W cm^{-2}, and confirms the non-conventional variation of collisional absorption which was also reported by quantum and classical kinetic models [43,44]. As $\alpha \propto \nu_{ei}$, the non-conventional increase of absorption can be qualitatively argued. At a very low temperature $T_e \to 0$ (or low intensity I_0), electrons do not have enough momentum to collide with ions, resulting in a vanishingly small ν_{ei} and α. As T_e and/or I_0 moderately increase, more electrons gain enough momentum to collide with ions and hence ν_{ei} and α increase with increasing T_e and/or I_0 which explains the increasing part of the absorption in figure 3 for $T_e < 15$ eV. After some higher threshold value of T_e and/or I_0 (i.e., $I_0 > I_c$), cross-section of electron–ion collision is gradually reduced (with v^{-3}) where both ν_{ei} and α start decreasing. From figure 3, it is inferred that for $T_e < 15$ eV, α increases with intensity up to $I_0 \approx 2 \times 10^{14}$ W cm^{-2}, and also for a fixed $I_0 \lesssim 10^{14}$ W cm^{-2}, α increases with increasing T_e up to $T_e \approx 15$ eV. However, there are discrepancies between PIC and analytical results at higher temperatures and higher intensities, which may be due to (i) time-varying field experienced by particles and (ii) movement of ion background to conserve momenta and energy during binary collisions in the PIC simulation as opposed to the analytical model where all particles experience the same peak laser field E_0 and ions remain stationary.

In analytical models of ν_{ei} (e.g., by Silin [31], Mulser *et al* [34] and Bornath *et al* [21]), distributions of electrons are assumed to be Maxwellian all the time during the laser interaction whereas in simulations this

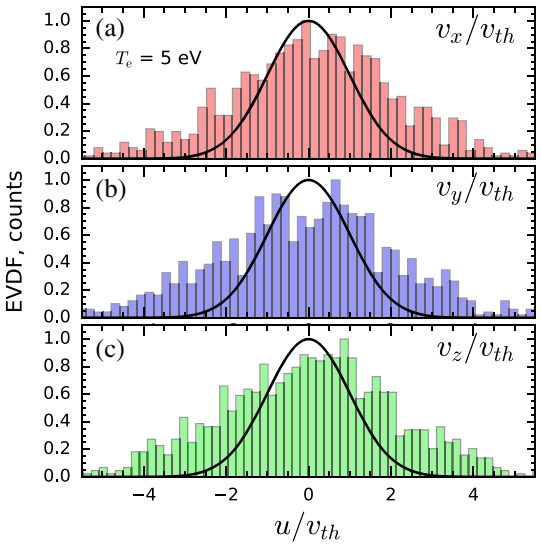

Figure 4. Distribution of velocity components ($u = v_x, v_y, v_z$) of electrons in units of v_{th} corresponding to the parameters of figure 2b at an intensity of 5×10^{14} W cm^{-2} just after the end of the simulation. Solid line is the expected Maxwellian with $T_{\text{e}} = 5$ eV.

assumption is often violated when electrons are dynamically driven by short laser pulse. Figure 4 shows distribution of velocity components ($u = v_x, v_y, v_z$) of electrons in units of thermal velocity corresponding to the parameters of figure 2b at an intensity of 5×10^{14} W cm^{-2} just after the end of the simulation. Solid line is the Maxwellian distribution corresponding to $T_{\text{e}} = 5$ eV. It is clearly demonstrated that velocity components do not strictly satisfy the Maxwellian distribution. Velocity distributions of electrons are also not isotropic which originate during the laser pulse driving. These differences, demonstrated by PIC simulation, from the idealistic analytical theory may also contribute to the deviation of the PIC result from the analytical estimate in figure 3. Nonetheless, non-conventional increase of collisional absorption is revealed in the low-temperature and low-intensity regime by the PIC simulation.

4. Summary

Collisional absorption of *s*-polarised laser light in a homogeneous, under-dense plasma is studied by a new particle-in-cell (PIC) simulation code considering one-dimensional slab-plasma geometry. To account Coulomb collisions between charge particles, a Monte Carlo (MC) binary collision scheme is used in the PIC code. For a given target thickness of a few times the wavelength of 800 nm laser, fractional absorption of light due to Coulomb collisions is calculated at different electron temperatures using a total velocity $v = (v_{\text{th}}^2 + v_0^2/2)^{1/2}$ dependent Coulomb logarithm $\ln \Lambda(v)$. In the low-temperature ($T_{\text{e}} \lesssim 15$ eV) and low-intensity ($< 5 \times 10^{14}$ W cm^{-2}) regime it is found that fractional absorption (α) of light non-conventionally increases initially with increasing intensity I_0 up to a maximum value corresponding to an intensity I_c, and then it drops approximately obeying the conventional scenario, i.e., $\alpha \propto I_0^{-3/2}$ when $I_0 > I_c$. Anomalous increase of α with I_0 was demonstrated in some earlier experiments [8,22], and recently explained by models [43,44] using total velocity-dependent cut-offs. Here, for the first time we report non-conventional variation of laser absorption by self-consistent PIC simulations assisted by Monte–Carlo collisions, thus bridging the gap between the models, simulations and experimental findings.

Acknowledgement

The author would like to thank Anshuman Borthakur for the initial help in the Monte–Carlo simulations and Sudip Sengupta for valuable suggestions.

References

[1] D R Bach, D E Casperson, D W Forslund, S J Gitomer, P D Goldstone, A Hauer, J F Kephart, J M Kindel, R Kristal, G A Kyrala, K B Mitchell, D B van Hulsteyn and A H Williams, *Phys. Rev. Lett.* **50**, 2082 (1983)
[2] U Teubner, J Bergmann, B van Wonterghem, F P Schäfer and R Sauerbrey, *Phys. Rev. Lett.* **70**, 794 (1993)
[3] D F Price, R M More, R S Walling, G Guethlein, R L Shepherd, R E Stewart and W E White, *Phys. Rev. Lett.* **75**, 252 (1995)
[4] M Cerchez, R Jung, J Osterholz, T Toncian, O Willi, P Mulser and H Ruhl, *Phys. Rev. Lett.* **100**, 245001 (2008)
[5] W Rozmus and V T Tikhonchuk, *Phys. Rev. A* **46**, 7810 (1992)
[6] Q L Dong, J Zhang and H Teng, *Phys. Rev. E* **64**, 026411 (2001)
[7] W L Kruer, *The physics of laser plasma interactions* (Addison-Wesley, New York, 1988)
[8] S Eliezer, *The interaction of high-power lasers with plasmas* (IOP Publishing, Bristol, 2002)
[9] Peter Mulser and Dieter Bauer, *High power laser–matter interaction, STMP 238* (Springer, Berlin, 2010)
[10] K R Manes, V C Rupert, J M Auerbach, P Lee and J E Swain, *Phys. Rev. Lett.* **39**, 281 (1977)
[11] P Mulser, D Bauer and H Ruhl, *Phys. Rev. Lett.* **101**, 225002 (2008)
[12] P Mulser and M Kanapathipillai, *Phys. Rev. A* **71**, 063201 (2005)

[13] P Mulser, M Kanapathipillai and D H H Hoffman, *Phys. Rev. Lett.* **95**, 103401 (2005)
[14] M Kundu and D Bauer, *Phys. Rev. Lett.* **96**, 123401 (2006)
[15] M Kundu and D Bauer, *Phys. Rev. A* **74**, 063202 (2006)
[16] M Kundu, P K Kaw and D Bauer, *Phys. Rev. A* **85**, 23202 (2012)
[17] I Kostyukov and J M Rax, *Phys. Rev. E* **67**, 066405 (2003)
[18] F Brunel, *Phys. Rev. Lett.* **59**, 52 (1987)
[19] H Cai, W Yu, S Zhu and C Zheng, *Phys. Plasmas* **13**, 113105 (2006)
[20] Th Bornath, D Kremp, P Hilse and M Schlanges, *J. Phys. Conf. Ser.* **11**, 180 (2005)
[21] Th Bornath, M Schlanges, P Hilse and D Kremp, *Phys. Rev. E* **64**, 26414 (2001)
[22] D Riley, L A Gizzi, A J Mackinnon, S M Viana and O Willi, *Phys. Rev. E* **48**, 4855 (1993)
[23] L Schlessinger and J Wright, *Phys. Rev. A* **20**, 1934 (1979)
[24] P Hilse, M Schlanges, Th Bornath and D Kremp, *Phys. Rev. E* **71**, 056408 (2005)
[25] J T Mendonça, R M O Galvão, A Serbeto, S-L Liang and L K Ang, *Phys. Rev. E* **87**, 063112 (2013)
[26] M Moll, M Schlanges, Th Bornath and V P Krainov, *New J. Phys.* **14**, 065010 (2012)
[27] G J Pert, *J. Phys. A* **5**, 506 (1972)
[28] G J Pert, *J. Phys. B* **8**, 3069 (1975)
[29] S Rand, *Phys. Rev.* **136**, B231 (1964)
[30] S-M Weng, Z-M Sheng and J Zhang, *Phys. Rev. E* **80**, 56406 (2009)
[31] V P Silin, *Sov. Phys. JETP* **20**, 1510 (1965)
[32] P Mulser and A Saemann, *Contrib. Plasma Phys.* **37**, 211 (1997)
[33] P Mulser and R Schneider, *J. Phys. A: Math. Theor.* **42**, 214058 (2009)
[34] P Mulser, F Cornolti, E Bésuelle and R Schneider, *Phys. Rev. E* **63**, 16406 (2000)
[35] H-J Kull and L Plagne, *Phys. Plasmas* **8**, 5244 (2001)
[36] J Wesson, *Tokamaks* (Oxford University Press, Oxford, 2004)
[37] G J Pert, *Phys. Rev. E* **51**, 4778 (1995)
[38] S C Rae and K Burnett, *Phys. Rev. A* **46**, 2077 (1992)
[39] P J Catto and Th Speziale, *Phys. Fluids* **20**, 167 (1977)
[40] D Kremp, Th Bornath, P Hilse, H Haberland, M Schlanges and M Bonitz, *Contrib. Plasma Phys.* **41**, 259 (2001)
[41] A Brantov, W Rozmus, R Sydora, C E Capjack, V Y Bychenkov and V T Tikhonchuk, *Phys. Plasmas* **10**, 3385 (2003)
[42] S Skupsky, *Phys. Rev. A* **36**, 5701 (1987)
[43] M Kundu, *Phys. Plasmas* **21**, 13302 (2014)
[44] M Kundu, *Phys. Rev. E* **91**, 043102 (2015)
[45] C K Birdsall and A B Langdon, *Plasma physics via computer simulation* (McGraw Hill, New York, 1981)
[46] R W Hockney and J W Eastwood, *Computer simulation using particles* (IOP Publishing, Adam Hilger, New York, 1988)
[47] Y Sentoku, K Mima, Y Kishimoto and M Honda, *J. Phys. Soc. Jpn* **67**, 4084 (1998)
Y Sentoku and A J Kemp, *J. Comput. Phys.* **227**, 6846 (2008)
[48] T Takizuka and H Abe, *J. Comput. Phys.* **25**, 205 (1977)
[49] T Takizuka, *Plasma Phys. Control. Fusion* **59**, 034008 (2017)
T Takizuka, K Shimizu, N Hayashi, M Hosokawa and M Yagi, *Nucl. Fusion* **49**, 075038 (2009)
T Takizuka, *Plasma Sci. Technol.* **13**, 316 (2011)
[50] S Ma, R D Sydora and J M Dawson, *Comput. Phys. Commun*. **77**, 190 (1993)
[51] R Lichters, R E W Pfund and J Meyer-ter-vehn, *A parallel one dimensional relativistic electromagnetic particle-in-cell code for simulating laser plasma interaction* (Max Planck Institute, Garching, Germany), http://www.lichters.net/work.html
[52] H Ruhl, Classical particle simulations, in: *Introduction to computational methods in many body physics* edited by M Bonitz, D Semkat (Rinton Press, 2006)
K Germaschewski, W Fox, N Ahmadi, L Wang, S Abbott, H Ruhl and A Bhattacharjee, *The plasma simulation code: A modern particle-in-cell code with load-balancing and GPU support*, http://arxiv.org/abs/1310.7866v1
[53] T Umeda, Y Omura, T Tominaga and H Matsumoto, *Comput. Phys. Commun.* **156**, 73 (2003)
[54] D M Sullivan, *Electromagnetic simulation using the FDTD method*, 2nd edn (Wiley-IEEE Press, London, 2013)
[55] G J Pert, *J. Phys. B* **38**, 27 (1999)
[56] B I Cohen, A M Dimits and D J Strozzi, *J. Comput. Phys.* **234**, 33 (2013)
[57] A Djaoui and A A Offenberger, *Phys. Rev. E* **50**, 4961 (1994)
[58] C D Decker, W B Mori, J M Dawson and T Katsouleas, *Phys. Plasmas* **1**, 4043 (1994)